Astronomy & Astrophysics

The GALEX Ultraviolet Virgo Cluster Survey (GUViCS)

V. Ultraviolet diffuse emission and cirrus properties in the Virgo cluster direction[⋆]

S. Boissier[1], A. Boselli[1], E. Voyer[1], S. Bianchi[2], C. Pappalardo[3,4], P. Guhathakurta[5], S. Heinis[6], L. Cortese[7], P.-A. Duc[8], J.-C. Cuillandre[8], J. I. Davies[9], and M. W. L. Smith[9]

[1] Aix-Marseille Université, CNRS, LAM (Laboratoire d'Astrophysique de Marseille) UMR 7326, 13388 Marseille, France
e-mail: samuel.boissier@lam.fr
[2] INAF-Osservatorio Astrofisico di Arcetri, Largo Enrico Fermi 5, 50125 Firenze, italy
[3] Centro de Astronomia e Astrofísica da Universidade de Lisboa, Observatório Astronómico de Lisboa, Tapada da Ajuda, 1349-018 Lisboa, Portugal
[4] Instituto de Astrofísica e Ciencias do Espaço, Universidade de Lisboa, OAL, Tapada da Ajuda, 1349-018 Lisboa, Portugal
[5] University of California Observatories/Lick Observatory, University of California Santa Cruz,
Department of Astronomy & Astrophysics, 1156 High Street, Santa Cruz, CA 95064, USA
[6] Department of Astronomy, University of Maryland, Stadium Drive, College Park, MD 20742-2421, USA
[7] Centre for Astrophysics & Supercomputing, Swinburne University of Technology, Mail H29 – PO Box 218, Hawthorn VIC 3122, Australia
[8] Laboratoire AIM, Service d'astrophysique, CEA-Saclay, Orme des merisiers, Bâtiment 709, 91191 Gif-sur-Yvette Cedex, France
[9] School of Physics and Astronomy, Cardiff University, The Parade, Cardiff, CF24 3AA, UK

ABSTRACT

Context. The Virgo direction has been observed at many wavelengths in recent years, in particular in the ultraviolet with GALEX. The far ultraviolet (FUV) diffuse light detected by GALEX offers interesting information on the large scale distribution of Galactic dust, owing to the GALEX FUV band sensitivity and resolution.
Aims. We aim to characterise the ultraviolet large scale distribution of diffuse emission in the Virgo direction. A map of this emission may become useful for various studies by identifying regions where dust affects observations by either scattering light or absorbing radiation.
Methods. We constructed mosaics of the FUV and near ultraviolet (NUV) diffuse emission over a large sky region (RA 12 to 13 h, Dec 0 to 20 deg) surrounding the Virgo cluster, using all the GALEX available data in the area. We tested for the first time the utilisation of the FUV diffuse light as a Galactic extinction $E(B-V)$ tracer.
Results. The FUV diffuse light scattered on cirrus reveals details about their geometry. Despite large dispersion, the FUV diffuse light correlates roughly with other Galactic dust tracers (coming from IRAS, *Herschel*, *Planck*), offering an opportunity to use the FUV emission to locate them in future studies with a better resolution (about 5 arcsec native resolution, 20 arcsec pixels maps presented in this paper) than for several usual tracers. Estimating the Galactic dust extinction on the basis of this emission allows us to find a smaller dispersion in the $NUV - i$ colour of background galaxies at a given $E(B-V)$ than with other tracers. The diffuse light mosaics obtained in this work are made publicly available.

Key words. ultraviolet: ISM – ultraviolet: galaxies – dust, extinction

1. Introduction

Large scale diffuse structures were found early-on in the Galaxy (de Vaucouleurs 1955). Sandage (1976) published the first detailed optical images of high latitude clouds found in a Galactic polar cap survey. However, it is only with the IRAS satellite that we were able to discover a rich geometry of far infrared emitting cirrus clouds over the full sky (Low et al. 1984). Deep optical imaging then revealed their emission due to dust scattering, showing good correspondence with the far infrared (e.g. de Vries & Le Poole 1985; Guhathakurta & Cutri 1994; Witt et al. 2008). The cirrus are also seen in the far ultraviolet (FUV) domain, in

which a major component of the light results from dust scattering (Witt et al. 1997).

Early studies of the FUV diffuse light can be found in Lillie & Witt (1976), Paresce et al. (1980), Jakobsen et al. (1984), Murthy et al. (1989, 1999), Fix et al. (1989), Hurwitz et al. (1991), Perault et al. (1991). Haikala et al. (1995) discovered Galactic cirrus directly from their FUV emission with the FAUST telescope. With the GALEX telescope and its All-sky Imaging Survey (AIS), extensive studies of the diffuse FUV emission became possible (e.g. Sujatha et al. 2010; Hamden et al. 2013; Murthy 2014).

Studying the cirrus in FUV is useful for many reasons:

– UV data allows the determination of the scattering dust properties in this wavelength domain, constraining dust grain properties (e.g. Witt et al. 1997; Sujatha et al. 2005).

[⋆] The diffuse light mosaics as FITS files are only available at the CDS via anonymous ftp to cdsarc.u-strasbg.fr (130.79.128.5) or via http://cdsarc.u-strasbg.fr/viz-bin/qcat?J/A+A/579/A29

- Recently, Seon et al. (2014) and Hodges-Kluck & Bregman (2014) have found ultraviolet haloes in edge-on galaxies that they interpret as reflection nebula from dust outside galaxies. While it is a different component than the cirrus themselves, characterising the dust properties in our backyard is also useful for such extra-galactic studies, provided the dust has a similar nature.
- Several works have found excess red emission (between 6000 and 8000 Å) in reflection nebulae, resulting from a luminescence excited by the FUV radiation of illuminating stars (Witt & Schild 1985). Guhathakurta & Tyson (1989), Guhathakurta & Cutri (1994), Gordon et al. (1998), Szomoru & Guhathakurta (1998), Witt et al. (2008) have shown that such extended red emission (ERE) is also found in the diffuse interstellar medium and cirrus clouds.
- The presence of cirrus in our Galaxy directly affects the colour or detection of objects in deep observations of extra-galactic sources, since cirrus modify the background to which the objects are contrasted. It is especially true for low surface brightness regions in nearby galaxies, such as tidal features that may be hard to distinguish from Galactic dust emission, or for lensing studies. This point is illustrated well by Fig. 10 in Duc et al. (2015).
- The presence of Galactic cirrus also affects UV/optical studies of extra-galactic sources via dust extinction (e.g. Burstein & Heiles 1982). Usually, data are simply corrected using Schlegel et al. (1998) maps based on the 100 microns dust emission.

Recently, a large area around the Virgo cluster has been surveyed at many wavelengths: especially by GALEX in the FUV and near ultraviolet (NUV) bands forming the GUViCS survey (Boselli et al. 2011). These data have already been used for several works that study the effect of the cluster environment on the evolution of galaxies (Cortese et al. 2011; Boselli et al. 2014), the effect of ram-pressure on star formation (Boissier et al. 2012), or stripped systems (Arrigoni Battaia et al. 2012). The source catalogues were publised in Voyer et al. (2014).

The area has also been observed in the framework of the Next Generation Virgo Cluster Survey (NGVS) in the optical (Ferrarese et al. 2012), of the *Herschel* Virgo Cluster Survey (HeViCS) in the far infrared (Davies et al. 2010), and of the Arecibo Legacy Fast ALFA survey (ALFALFA) in HI (Giovanelli et al. 2005). Deep *B* and *V* images (reaching 28.5 mag arcsec^{-2} in the *B* band) were obtained by Mihos et al. (in prep.) in about 15 deg^2 around M87 and M89, using the Schmidt telescope at Kitt Peak. While several of these surveys are mostly dedicated to extra-galactic science, they can also be used to study the cirrus component in our Galaxy or may be affected by them.

In this paper, we concentrate on the UV data from the GUViCS survey. We characterise the cirrus in the UV and compare our findings to other wavelengths. Recently, Hamden et al. (2013) have performed a full sky study of the ultraviolet diffuse light in the GALEX All sky Imaging Survey. We focus instead on the Virgo cluster area, taking advantage of all the observations performed that allow us to use deeper data, to visually inspect FUV detected cirrus, and to compare them to ancillary data in a small region of the sky, while their work is statistical in nature. This will be useful for any analysis based on deep data (from the many recent surveys of Virgo) that may be subject to pollution by diffuse low surface brightness emission. For instance, our FUV maps have already been used by Durrell et al. (2014)

to make sure their results for the spatial distribution of globular clusters in Virgo were not affected by cirrus.

The presence of cirrus may be crucial in the study of low surface brightness features that may be associated to tidal interactions, expected to be frequent in the cluster environment of Virgo. A school case is the interacting pair NGC 4435/4438. Cortese et al. (2010) studied this system with a combination of multi-wavelength data including far infrared and FUV observations. These data helped them to elucidate the nature of a "plume" detected in deep optical data. The cirrus are also easily recognised in a simple visual examination of the deep optical imaging of Mihos et al. (in prep.). While they seem to correspond well to the location where we detect them in FUV or infrared, a detailed analysis (distinguishing the cirrus vs. faint emission linked to the galaxies and comparing to other wavelengths) will be performed in the future.

In Sect. 2, we present our data and explain how we constructed the mosaics (made publicly available with this paper) over a large sky area (RA 12 to 13 h, Dec 0 to 20 deg) surrounding the Virgo cluster. An analysis (UV properties of cirrus, comparison with other wavelengths) is done in Sect. 3, and our conclusions are summarised in Sect. 4

2. The GUViCS mosaics

2.1. FUV and NUV GALEX mosaics

The GUViCS survey was presented in Boselli et al. (2011). It combines a large number of tiles observed with GALEX in the FUV and NUV bands (with effective wavelengths of 1528 and 2271 Å, respectively, and spatial resolution of about 5 arcsecs). The minimal exposure time observed corresponds to the AIS survey (exposure times of typically 100 s, reaching a surface brightness of about 26 mag arcsec^{-2}), but are often typical of the Medium Imaging Survey or Nearby Galaxy Survey (1500 s exposure times, 28 mag arcsec^{-2}). A few tiles have even much deeper data because they were observed for other purposes and are included in GUViCS. An update with all the tiles we include in our work and several source catalogues can be found in Voyer et al. (2014). The circular ~1.2 deg diameter field of GALEX offers a good basis for mapping large-scale structures. However, Galactic cirrus extend beyond this size. To circumvent this difficulty, we took advantage of having access to all the files needed to generate mosaics of the full area of the GUViCS survey in both the FUV and NUV bands of the GALEX telescope.

We started from the following GALEX pipeline products: intensity maps, exposure maps, and object detection masks. After some tests, we decided to truncate them at a radius of 0.58 deg to avoid the problems often observed on the edge of GALEX fields (i.e. increased noise, elongated point-spread function). We also removed a few tiles originally in the survey but with obvious positioning problems (see Voyer et al. 2014, for examples).

As a first step, in all the tiles, we replaced pixels in the object detection maps by surrounding values. Then, we used the Montage software[1] to co-add the object-subtracted intensity maps by weighting each image by its exposure time. Montage allows the final image to be projected on an arbitrary pixel grid. We tested several resolutions looking for a balance between resolution and signal-to-noise. In this paper, we present maps of a mosaic with 1 arcmin sized pixels over the full Virgo area for tiles from the AIS (with advantage of being homogeneous

---

[1] `http://montage.ipac.caltech.edu/`

and covering the largest possible area). We also produced an image with pixels of 20 arcsecs size showing finer details in the background structure owing to deeper exposures (i.e. exposure times of at least the 1500 s typical of the GALEX Medium Imaging Survey).

This method is similar to the one used in Hamden et al. (2013). The main differences are that they rely on sky background images from the GALEX pipeline, while we replace the detected objects within the masks by neighbouring pixel values by ourselves (the pipeline background is smoothed and may not reproduce small-scale variations in the background). Second, they grow the masks of detected objects to limit the pollution of data by actual objects, while we keep the masks at their size to increase our chance of seeing real structures (even if the absolute flux level may in some cases be polluted). Finally, their final map has pixels covering 11.79 arcmin^2, while we choose 1 arcmin^2 and 20×20 arcsec^2 pixels in our study of a more limited area. The higher resolution allows us to see details of the structures revealed in the FUV with deeper data than the All Sky Imaging Survey, which they use in their full sky statistical study.

The FUV mosaics obtained in this way presented a few artefacts of the absence of data in a small area on the edge of the FUV detector. We manually edited the FUV mosaics to interpolate over such regions. During this visual inspection, we also manually masked a few sources that had been badly subtracted (usually very bright stars or extended galaxies). These corrections only concern a few pixels. We checked that they do not affect the conclusions presented here by performing our analysis with both the raw mosaic and the edited image. The only visible difference is a tail of FUV-bright pixels that correspond to badly subtracted objects in the uncorrected map.

As a final step, to obtain smoother maps, we found it useful to median-filter our mosaics in 3×3 pixel boxes. This alleviates the potential difficulties linked to the choice of the pixel grid origin, and it reduces the noise at the very low surface brightness of the cirrus, at the price of degrading the resolution of our mosaic further to about 3 arcmin (for the lower resolution mosaic). This is the same order of magnitude as the resolution of the other dust tracers to which we compare our map.

2.2. Units

Different communities express the UV surface brightness in different units (see Leinert et al. 1998, for an exhaustive list of surface brightness units and their conversions). To make it easy to convert between various units used in this paper, we express most of our maps in GALEX counts (per sec). To have graspable numbers, we used counts per arcmin^2 in most cases. When FUV/NUV comparison was involved, we switched to AB magnitudes and surface brightnesses which are relatively standard. Conversion between counts and surface brightness is straightforward[2]:

$$\text{FUV AB magnitude } = -2.5\log 10\,(\text{counts s}^{-1}) + 18.82 \quad (1)$$

$$\text{NUV AB magnitude } = -2.5\log 10\,(\text{counts s}^{-1}) + 20.08. \quad (2)$$

"Continuum Units" (CUs, photons cm^{-2} s^{-1} sr^{-1} Å^{-1}) are often used in studies of the FUV diffuse light. It is straightforward to convert from counts to CUs for the FUV GALEX band:

$$\text{counts s}^{-1}\,\text{arcmin}^{-1} = \text{CUs}/1260. \quad (3)$$

2.3. Other wavelength maps

Large scale variations in the sky background are known to be related to zodiacal light and cirrus. These components are often studied by looking at their emission in the far infrared. Schlegel et al. (1998) produced maps of IRAS/COBE 100 μm emission that have been widely used. The IRAS data were reprocessed by Miville-Deschênes & Lagache (2005) to obtain a slightly improved angular resolution (4.3 arcmin) at 100 microns and better calibration by taking the time and brightness response of the detector into account. This improved map is called IRIS (Improved Reprocessing of the IRAS Survey). Planck Collaboration XI (2014), however, mention that the zodiacal light subtraction was done differently in the IRIS project with respect to Schlegel et al. (1998) and proposed a simple correction to use the large scale variations from Schlegel et al. (1998) and the small-scale variations from Miville-Deschênes & Lagache (2005). We have used the IRIS 100 micron map and adopted the same correction in our study. Finally, we prepared a mask with all VCC galaxies detected by IRAS and with some other bright objects, such as known field galaxies and stars. The mask excludes up to twice the 100 microns IRAS resolution around each source. Masked regions were interpolated over.

The Planck collaboration has used IRAS and *Planck* all sky maps to compute the properties of the Galactic dust thermal emission. The collaboration made the dust maps available, including dust opacity, temperature, and radiance (Planck Collaboration XIX 2011; Planck Collaboration XI 2014). The dust radiance was converted into a reddening $E(B - V)$ map[3] using the colours of SDSS quasars as a reference. This map should be adequate to estimate the dust attenuation for extra-galactic sources with a spatial resolution of about 5 arcmin.

The HeViCS project (Davies et al. 2010) collected *Herschel* data in four fields within the area studied in this paper. In this work, we have used the 250 μm maps observed with the SPIRE instrument (spatial resolution of about 18 arcsecs). The data was reduced using the *Herschel* dedicated software HIPE, adopting the v11 calibration tree, assuming the gain correction for extended sources, and combining the scans with the built-in destriper. This was found to preserve the large scale diffuse emission better than the dedicated pipeline used in other HeViCS works, which was tailored for extra-galactic targets (see e.g. Auld et al. 2013). Further details on the data reduction, together with a study of the properties of the diffuse cirrus emission will be presented in Bianchi et al. (in prep.). We interpolated these maps over the same mask as the one used for the IRAS 100 micron emission. After this step, however, the HeViCS tiles were still filled with many faint sources. The background was thus determined following the same procedure as in Pappalardo et al. (2015), i.e. iteratively computing a background with SExtractor. The cirrus are very visible in HeViCS images. Baes et al. (2014) discuss their role as potential non-extra Galactic sources in their cross-correlation of HeViCS and *Planck* maps. A HeViCS study of the cirrus is in preparation (Bianchi et al., in prep.), so the HeViCS findings are not discussed here in detail, but the data are shown for illustrative and comparison purposes.

We extracted the parts of the 100 micron and $E(B - V)$ *Planck* maps that cover our UV mosaics using the Aladin sky atlas (Bonnarel et al. 2000). The 250 micron maps come directly from the HeViCS collaboration. All were registered to the same pixel scale as our various UV maps (1 arcmin and 20 arcsec).

---

[2] http://galexgi.gsfc.nasa.gov/docs/galex/FAQ/counts_background.html

[3] http://irsa.ipac.caltech.edu/data/Planck/release_1/all-sky-maps/

It would be very interesting to compare the ultraviolet detection of cirrus to the all-sky dust emission computed in the WISE W3 band by Meisner & Finkbeiner (2014). At 12 microns, this map reveals the emission from small grains and polycyclic aromatic hydrocarbon (PAHs) absorbing mostly radiation in the ultraviolet. Scattered ultraviolet light should then spatially occur close to the 12 microns emission (while the thermal dust is heated by the general interstellar radiation field that can be spatially mismatched from the ultraviolet strong sources). We did download the dust emission maps published by Meisner & Finkbeiner (2014). Sadly, the Virgo area is crossed by a wide stripe of corrupted data, making the maps unusable for a statistical comparison that would correspond to our goals. A detailed comparison of some regions could still be possible in the future (we illustrate this point in Sect. 4).

3. Analysis of large scale variations

3.1. Zodiacal light

For general studies of the zodiacal light in the UV, the reader is invited to consult Frey et al. (1977) and Murthy (2014), among others. Here we only analyse how it affects on our mosaics and their contamination on the cirrus emission. In the NUV band, we found that our object-subtracted map presented a strong gradient in its background, which can be ascribed to the zodiacal light. The GALEX site proposes a zodiacal light tool[4] based on the zodiacal light study by Leinert et al. (1998). It predicts the level of zodiacal light expected for a position and an epoch. We checked with this tool that indeed a decreasing gradient is expected in the NUV observations along the ecliptic latitude.

We show in Fig. 1 the actual gradient with ecliptic latitude that we measured in our GALEX diffuse NUV image over the full Virgo cluster area. It is compared to the prediction of the GALEX zodiacal tool for a few coordinates that regularly cover the area, when adopting the date of January 1. Variations with the date do occur, but change in the same way at all latitudes. These variations are usually lower than about 25 percent, except during a zodiacal emission spike, when GALEX observations were not executed. At low ecliptic latitude, we find high values of the background, which is consistent with the GALEX tool model. At a higher latitude, our background decreases, as the model does, but by a smaller amount. This may be due to either an underestimation of the zodiacal light model or a contribution to the background by other sources (ghosts of stars, artefacts, etc.). We note, however, that if the background was dominated by other sources, it should not depend on the latitude. Figure 1 shows the gradient that we determined by hand to approximatively pass by the darkest regions within the map at different latitude. This gradient is only used in the next section to consider the cirrus NUV detection and in Fig. 4.

We proceeded to the same exercise in FUV (Fig. 2). In this case, the expected level of the zodiacal light is extremely low. The observed level is much higher than the prediction and is independent of the latitude (as found by Hamden et al. 2013, on a larger scale). Other effects thus dominate the background (e.g. ghosts, residuals from subtracted objects, unresolved distant sources, and Galactic cirrus studied in the following).

We also looked at how the diffuse FUV and NUV background counts vary with the Galactic latitude. We found no trend with the Galactic latitude in FUV, but we did investigate a limited range of Galactic latitude above 55 deg, while most of the trend
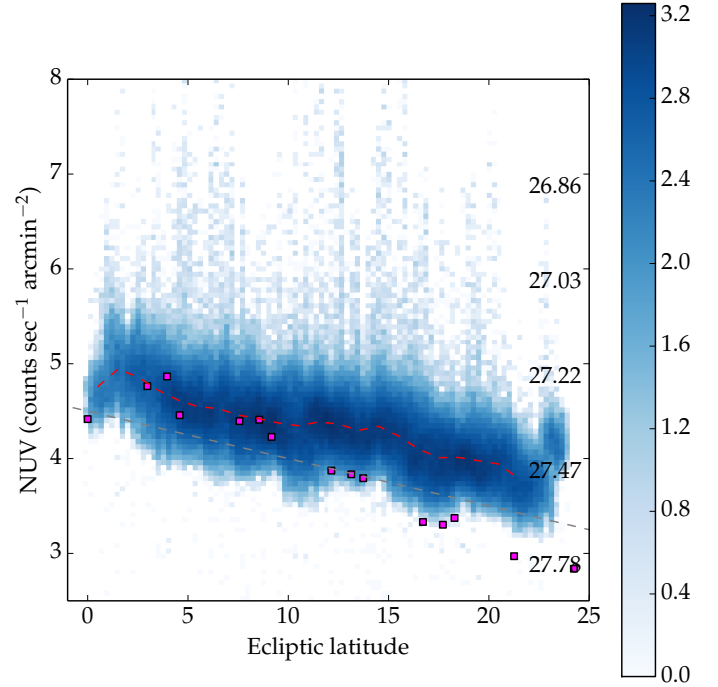
---

4 http://sherpa.caltech.edu/gips/tools/zlct.html

Fig. 1. Object-subtracted NUV counts (based on 1 arcmin pixels, median-filtered in 3×3 pixel boxes) as a function of the ecliptic latitude. The numbers on the right axis indicate the surface brightness in units of AB magnitude per square arcsec. The colour bar indicates the decimal logarithm of the number of pixels per 2D bin. The red line shows the average. The grey line is the adopted background (Sect. 3.2). The magenta squares report predictions of the GALEX zodiacal light tool.
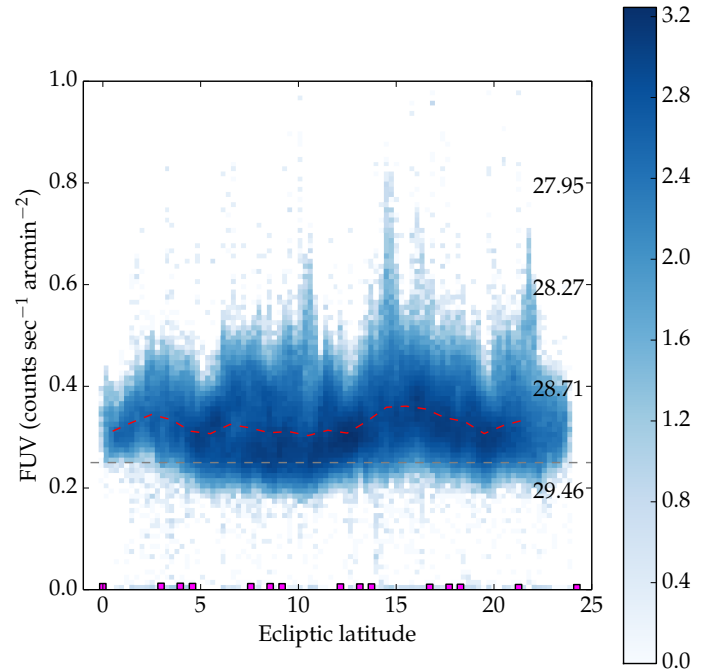

Fig. 2. Object-subtracted FUV counts (based on 1 arcmin pixels, median filtered in 3×3 pixels boxes) as a function of the ecliptic latitude. The numbers on the right axis indicate the surface brightness in units of AB magnitude per square arcsec. The colour bar indicates the decimal logarithm of the number of pixels per 2D bin. The red line shows the average. The grey line is the adopted background (Sect. 3.2). The magenta squares report predictions of the GALEX zodiacal light tool.
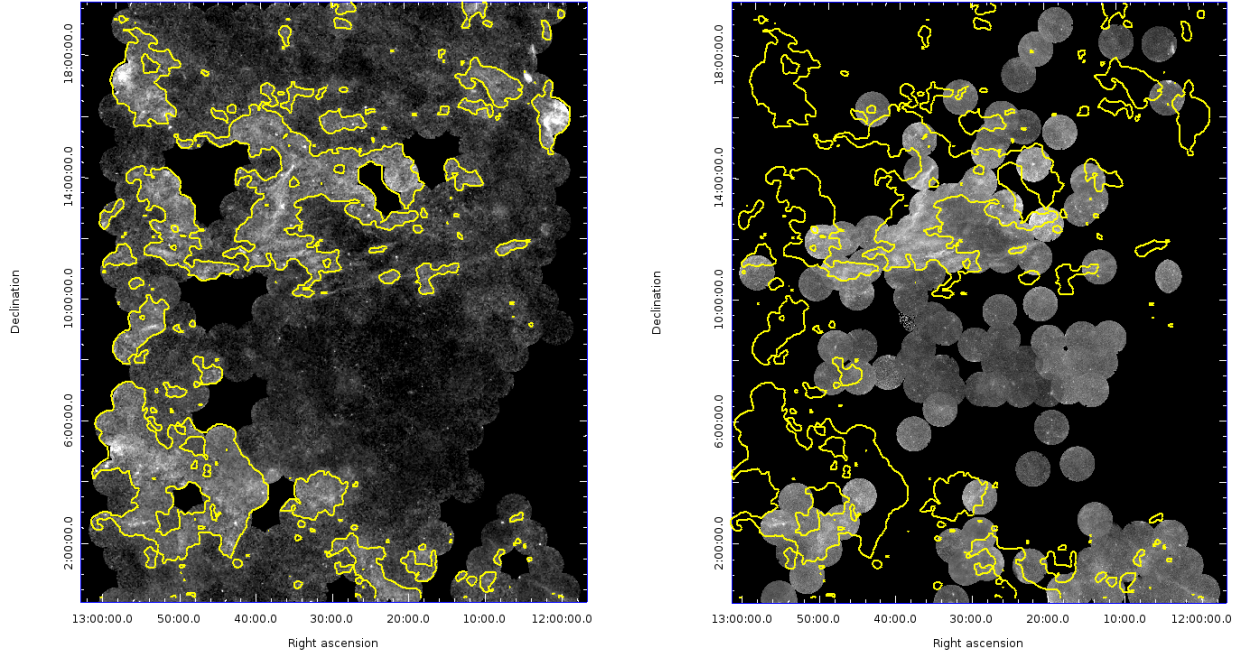
Fig. 3. *Left*: mosaic showing the diffuse FUV emission obtained from AIS data (1 arcmin pixels, median smoothed on 3 × 3 pixels). *Right*: diffuse FUV emission obtained on the basis of deeper data (on 20 arcsec pixels, median smoothed on 3 × 3 pixels). The contours indicate roughly the regions in which the cirrus emission is found (Sect. 3.2).

due to cirrus is expected to occur at lower latitudes (Hamden et al. 2013). An anti-correlation is found in the NUV background counts, but we interpret it as the result of the variation with the ecliptic latitude (the zodiacal light described above), since in our field, the Galactic and ecliptic latitudes vary in the same direction.

3.2. Ultraviolet cirrus detection

In the FUV, we measured the background level in several regions in the darkest area of the sky in our mosaic. We did this by using the IRAF task IMEXAMINE in several rectangular regions in a similar manner to previous works with GALEX data (e.g. Boissier et al. 2007, 2008, 2012). As can be surmised from Fig. 2, this background is found at a level of 0.25 counts per sec per arcmin^2 (with a 0.11 3σ uncertainty per pixel). We created a FUV background-subtracted map by subtracting this constant value to the FUV mosaic. By proceeding this way, we basically remove any emission not related to the cirrus themselves, which could be due to air glow or extra-galactic sources and which should correspond to the "offset" observed by Hamden et al. (2013). We acknowledge that this background could include a very diffuse cirrus contribution that is then subtracted in our approach. The nature of this diffuse component emission is still unknown and the subject of several studies (see e.g. Henry et al. 2015, who test the hypothesis of a dark-matter interaction with the interstellar medium, or of small dust grains; and references therein).

The remaining FUV emission above this constant background is assumed to be due to cirrus. It is true that some part of it could have other sources (extended haloes of galaxies, tails, or streams, intracluster light) but the result discussed in the rest of the paper seems to be consistent with this emission being dominated by the Galactic cirrus. We created a detection map by adopting a 3σ threshold above this level. This

map was then smoothed (by a Gaussian filter of 6 arcsec) with the only goal to compute contours (in ds9) at a single level (0.1 counts s^{-1} arcmin^{-2}) in order to roughly identify the cirrus regions geometrically. These contours are not directly used in the science analysis of this paper, but we overlay them in our figures. They are shown in Fig. 3 over the FUV mosaics obtained from AIS data and from deeper GUViCS data.

In the NUV, we first constructed a background map to reproduce the gradient observed in Fig. 1. We used the darkest regions to estimate its zero point. This background was subtracted to the NUV image. We then inspected the sky level within this background-subtracted image and found it to be flat. Measuring the sky level in dark regions, we obtained the value of 0.1 counts per sec per arcmin^2 with a 3σ value of 0.52: it is consistent with zero, demonstrating that the sky gradient subtraction procedure performed well. We then produced a NUV "detection map", by adopting a threshold at this 3σ value also here.

3.3. UV properties of Galactic cirrus

Figure 4 (top left) shows the background-subtracted images in NUV and FUV with the FUV detection contours. The comparison definitively shows the blue colour of the cirrus with respect to the background. To characterise the UV properties of our cirrus, we show in Fig. 5 the relation between the FUV-NUV colour and the FUV surface brightness, obtained from the object-subtracted, background-subtracted 3 × 3 median-filtered 1 arcmin size pixel maps. The higher resolution maps (having a higher signal-to-noise, but smaller and inhomogeneous coverage) produce very similar results from this point of view. Our data point to bluer colours for brighter surface brightnesses. Sujatha et al. (2010) find such an increase in the FUV/NUV ratio that they interpreted as a sign of fluorescent emission of molecular hydrogen. In our data, however, we cannot rule out a detection issue, as can be seen from Fig. 5. Taking the thresholds
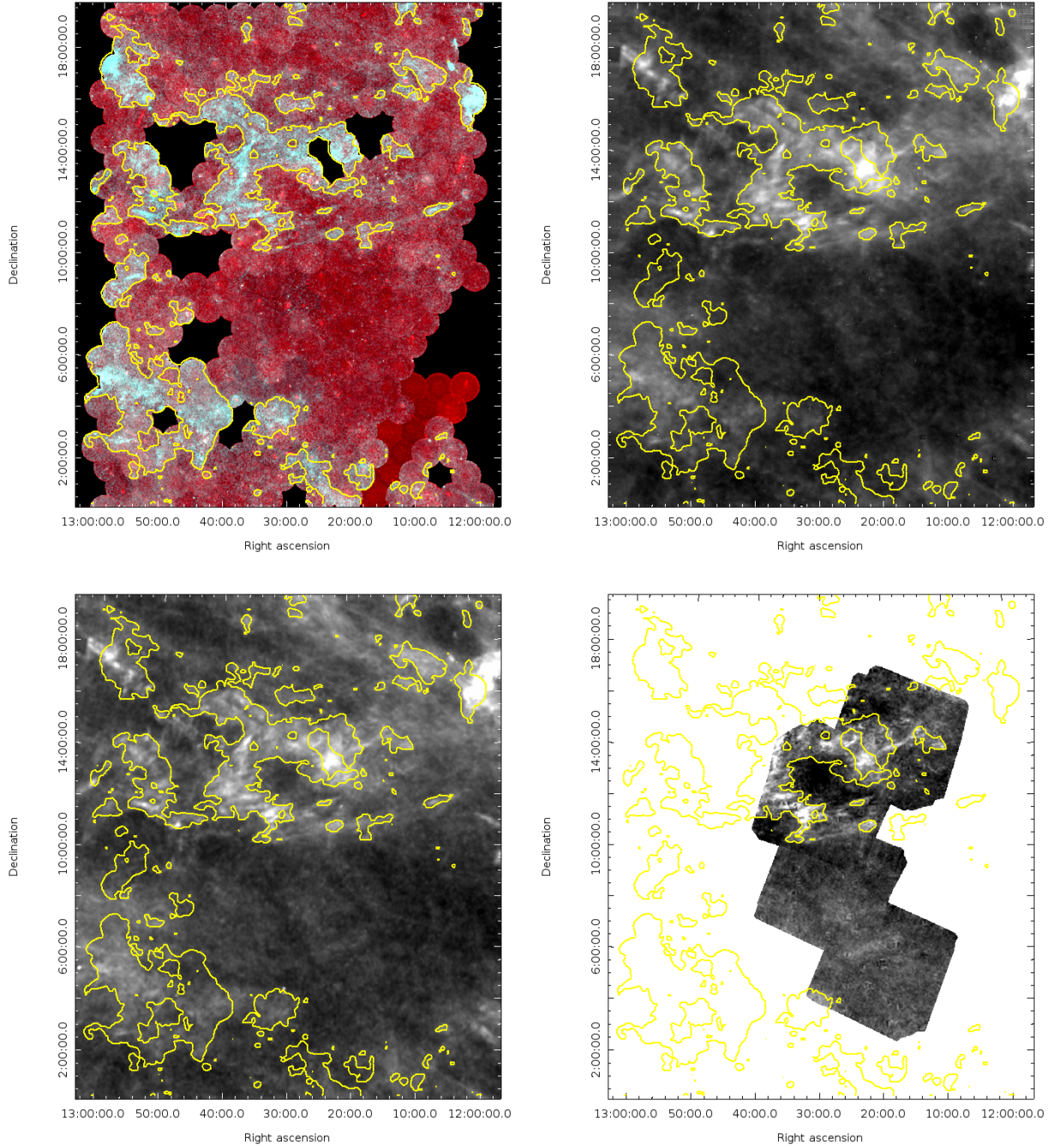
Fig. 4. Gallery of multi-wavelength tracers of the cirrus in the Virgo Area. *Top left*: composition of FUV (blue) and NUV (red) mosaics from GUViCS. *Bottom left*: *Planck* $E(B − V)$ map. *Top right*: 100 microns IRIS map. *Bottom right*: 250 microns HeViCS map. The yellow contours are the broadly defined regions of cirrus detected in FUV (Sect. 3.2).

discussed in Sect. 3.2 into account and restricting ourselves to the pixels where the signal-to-noise is higher than three at both wavelengths, we find that the typical FUV-NUV colour of the cirrus is close to 0. This is very similar to the colour of $FUV − NUV ∼ 0.11$ that can be deduced from the spectral distribution found by Gondhalekar et al. (1980) for the interstellar radiation field, probably typical of B-stars illuminating the dust clouds. In the scattered haloes of external star-forming galaxies, Hodges-Kluck & Bregman (2014) also found quite blue colours with spectral energy distributions (λF_λ) that are flat (or declining from FUV to NUV), corresponding to a FUV-NUV colour of ∼0.4 (or bluer).

3.4. Comparison to other wavelengths

Figure 4 shows the 100 microns, 250 microns, and *Planck* dust-reddening maps compared to a FUV+NUV combination (obtained from the shallow data covering a large fraction of the full area). In general, a similar morphology is found with the various tracers. This sort of agreement between various indicators for the cirrus presence has already been discussed before by, for example, Guhathakurta & Cutri (1994) for the optical, 100 micron, and gas distributions or Seon et al. (2011) for relations between FUV, gas column density, and 100 micron radiation. The agreement between the various tracers is, however, not perfect. For
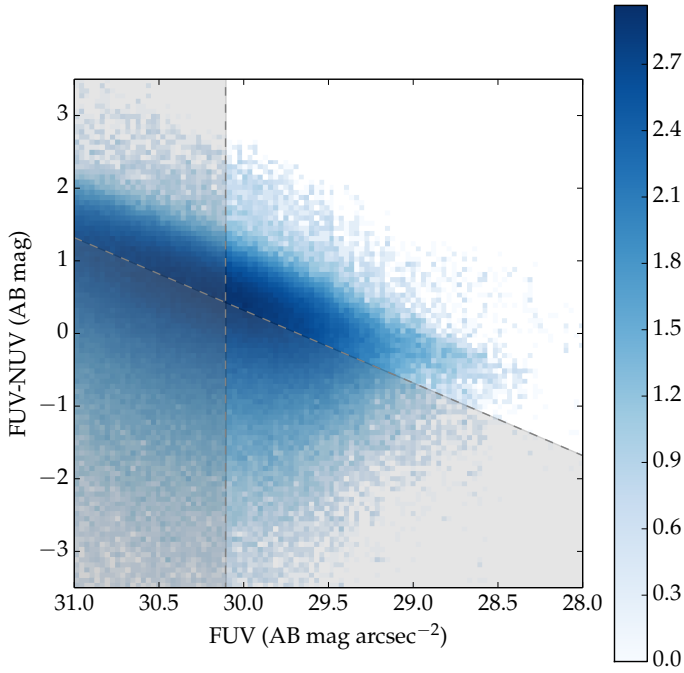
Fig. 5. FUV-NUV colour as a function of surface brightness (based on the 1 arcmin pixel-size mosaics). The lines shows our detection thresholds in FUV and NUV (shaded area are below the detection threshold and thus subject to large uncertainties). The colour bar indicates the decimal logarithm of the number of pixels in each 2D bin.

instance, some regions of the *Planck* $E(B - V)$ or far infrared maps are dark within the UV contours in Fig. 4 (e.g. around 12 h 55 m, 9 deg). Small scale variations bring clues about the physical properties of the dust (Guhathakurta & Cutri 1994) even if another source of dispersion is caused by the anisotropic interstellar radiation field and the precise geometry of dust and bright stars (Witt et al. 1997; Seon et al. 2011). It is beyond the scope of this paper to explore these aspects in detail here, but the maps that we distribute may help for doing these studies in the future.

We show in Fig. 6 a comparison of several dust tracers in a region for which we do have data deeper than the AIS, using our 20 arcsec pixel map. It reveals that the UV allows following the structure of the cirrus in detail with better resolution than the traditional tracers.

Beyond a simple visual comparison of the maps, we now proceed to a quantitative comparison, pixel by pixel, of the FUV cirrus emission and other dust tracers. Figures 7 and 8 show the distributions of pixels, and Table 1 provides the correlation coefficients between the FUV and other dust tracers pixels.

A relation between FUV and 100 micron emission has been reported in several studies (Perault et al. 1991; Witt et al. 1997; Sasseen & Deharveng 1996). We show the relation we find in the Virgo direction in Fig. 7. The relation found by Hamden et al. (2013) on larger scales seems to holds on our 1 arcmin scale, with a 3 × 3 pixel median filter (an adequate pixel size taking into account the 100 microns resolution). In this comparison, we used only the slope of the 100 micron-FUV relation of Hamden et al. (2013) since the intersect is believed to be due to uniform sources that we subtracted in our map construction. We adopt their slopes in the Galactic latitude ranges corresponding to Virgo (60−75 and 75−90). The good agreement suggests that our background measurement and subtraction were efficient. On the other hand, we note an important dispersion, which is a

Table 1. Pearson correlation coefficients.

X variable	Y variable	Correlation coefficient (Pearson)
FUV	100 microns	0.57
FUV	250 microns	0.47
FUV	$E(B - V)$ *Planck*	0.61

sign that the dust emission in the far infrared and the FUV reflection on dust do not coincide perfectly. We found a similar relation between the FUV and the 250 micron emission, albeit with more dispersion. The 250 map, however, covers only a part of our FUV data.

The dispersion in the relation between the FUV and infrared pixel values (reflected by the relatively poor correlation coefficients) is most likely because while the two tracers generally trace the shape of the cirrus, they are more complementary than equivalent. This can be seen better in Fig. 9, where we show the ratio of the FUV diffuse emission to the IRIS 100-micron emission. We first applied a 6 arcmin Gaussian convolution to each image to reveal the differences on large scales, which avoided their being dominated by small scale fluctuations (or resolution effects). It is evident from this figure that this ratio is not identical in the field but varies with position. It is not only due to noise since it varies also within the contours, indicating regions where FUV is definitively detected. Figure 10 shows a zoom in a region where a clear elongated cirrus structure is seen, where part of it is obvious through its FUV emission, part of it through its far infrared emission. Some of the mismatch could be due to the relative geometry of stars and various type of dust. The FUV scattered light may occur on small grains predominantly in regions close to FUV emitting stars, while the far infrared radiation corresponds to the thermal emission of the dust heated by the interstellar radiation field, heating that can also occur in the absence of the hottest stars in the immediate vicinity.

3.5. FUV as a dust tracer in the Virgo Cluster area

We show the distribution of pixels in the FUV emission vs. Planck Collaboration XI (2014) $E(B - V)$ extinction plane in Fig. 8. The two variables are correlated. A very similar trend is obtained on the basis of the Schlegel et al. (1998) maps. (The figure includes the best linear fit in this case.) This indicates that the FUV diffuse emission is at least loosely linked to the extinction as measured through the dust emission. We quantitatively explore the link between the FUV diffuse emission and the extinction in this section. The FUV map used is the 1 arcmin pixel one, which has been median-smoothed over 3 × 3 pixels. The *Planck* extinction map has a resolution of a few arcmin, so this scale is pertinent for our comparison. (We did, however, compute the distribution at higher resolution – with the 20 arcsec pixels map – and found very similar trends.) Some scatter is found, as expected, since the FUV and the *Planck* maps do not correspond perfectly to each other. The figure, however, suggests a clear average relation between the two quantities. We computed averages within bins of FUV emission and performed a simple fit to these values to find

$$E(B - V) = 0.02378 + 0.1105 \times FUV \left(\text{counts s}^{-1} \text{ arcmin}^{-2} \right). \quad (4)$$

A shallower slope (∼0.09 instead of 0.11) is found if the Schlegel et al. (1998) map is used rather than the Planck Collaboration XI (2014) one. Considering the dispersion, the value of this slope is uncertain, but a correlation is clearly present. Assuming the
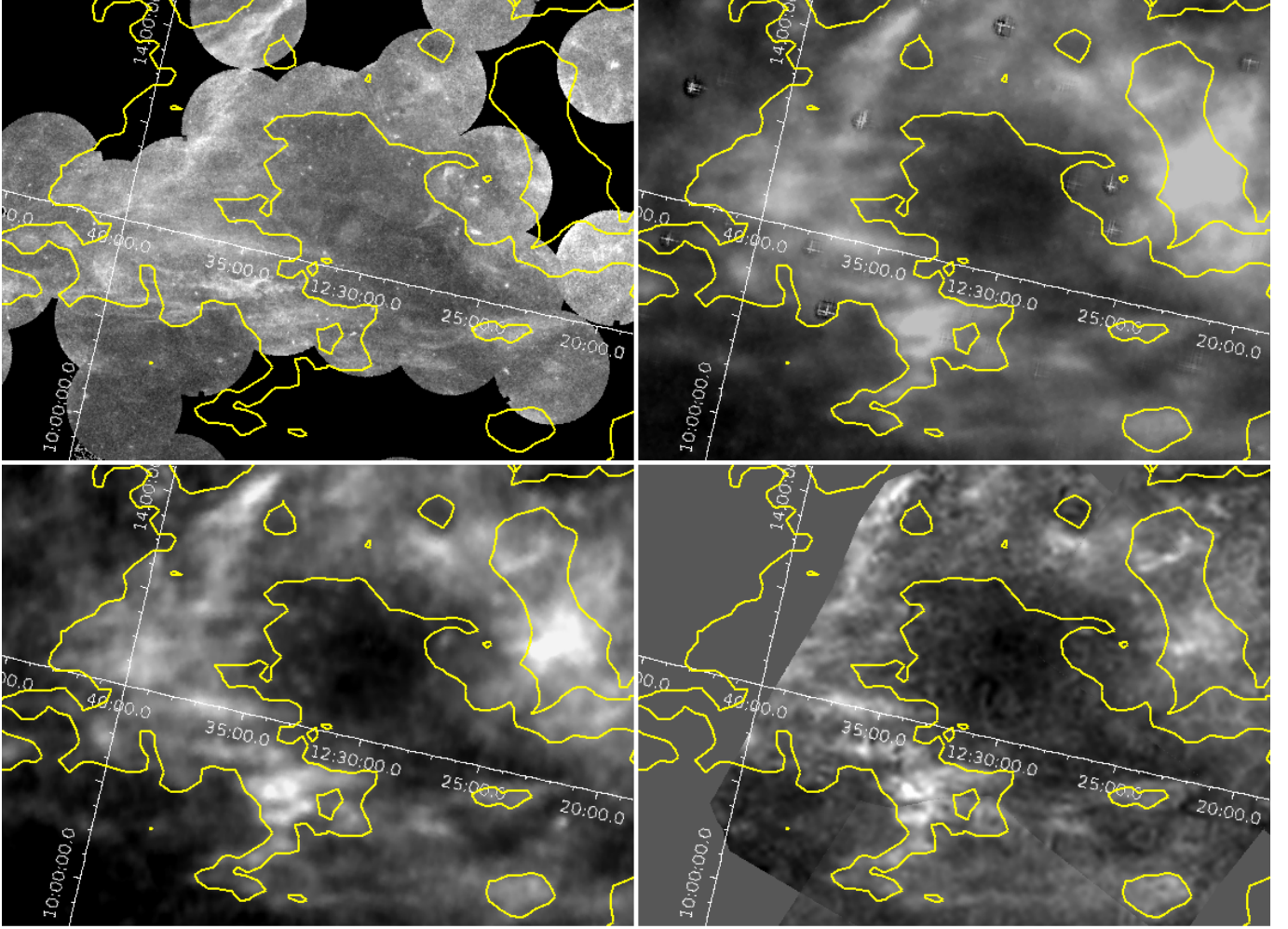
Fig. 6. Comparison of several cirrus indicators in a zoomed region with deep FUV data (*top left*). This map is compared with the 100 microns IRIS map (*top right*), HeViCS 250 microns (*bottom right*), *Planck* $E(B - V)$ map (*bottom left*).

underlying average relation between FUV emission and dust extinction holds on small scales, we invite any researcher working in the Virgo area to use our distributed 20 arcsec (or 1 arc-min) map and this relation to predict "alternative" extinction values with respect to the traditional Schlegel et al. (1998) ones (or *Planck* ones). The advantage is that these FUV maps reveal detailed structures of the cirrus that are not visible in the long-wavelength maps (lack of resolution/sensitivity, and complementarity: see Sect. 3.4). We warn the reader, however, that a one-to-one relation is not expected because the FUV emission is sensitive to the geometry of dust and UV-emitting stars (Witt et al. 1997; Seon et al. 2011). Equation (4) should then be used with caution, especially for individual objects. Despite this drawback, we believe that an attenuation computed from our FUV diffuse maps provides an alternative value for the reddening that may be complementary to traditional dust tracers.

3.6. Testing the FUV extinction determination with an extra-galactic catalogue

To test this new extinction estimation, we used background galaxies detected in NUV with the GUViCS catalogue from Voyer et al. (2014). The idea of using background objects to study Galactic extinction is not new (Burstein & Heiles 1978) and was applied by Fukugita et al. (2004) to SDSS data. In fact, the $E(B - V)$ Planck Collaboration XI (2014) map is based on

this idea because the colours of background quasars were used to calibrate the relation between $E(B - V)$ and the thermal dust emission. Cuillandre et al. (2001) applied a similar method to measuring attenuation in M31 from background galaxies. They also explored the effect of attenuation on their colour and found it to be hard to detect. In our case, however, the used colour is more favourable because we expect a stronger effect, using the NUV band, which is very sensitive to extinction.

We did not determine the extinction from the galaxy counts, but rather verified that the colours of background galaxies statistically agree with the Galaxy dust reddening at their position. In Fig. 11, we show the trend between the $NUV - i$ colour and reddening for Virgo and background galaxies, with a signal-to-noise that is higher than ten in the Voyer et al. catalogue, leaving us with around 25 000 galaxies (similar results are obtained when the minimum signal-to-noise is reduced to 2, with about 70 000 objects). This number is of course much larger than the number of quasars in the same region. The galaxy colour is taken directly from the catalogue. The figure shows the average and the dispersion of the colour of galaxies in various bins of Galactic reddening. We show four cases depending on which reddening is used: the one from the Schlegel et al. (1998) maps, given in the catalogue; the one from the *Planck* $E(B - V)$ map; or the one derived from the FUV maps (the 1 arcmin and 20 arcsec pixel ones) when applying Eq. (4). In all cases, the average colour becomes redder (with a broad dispersion) with the reddening.
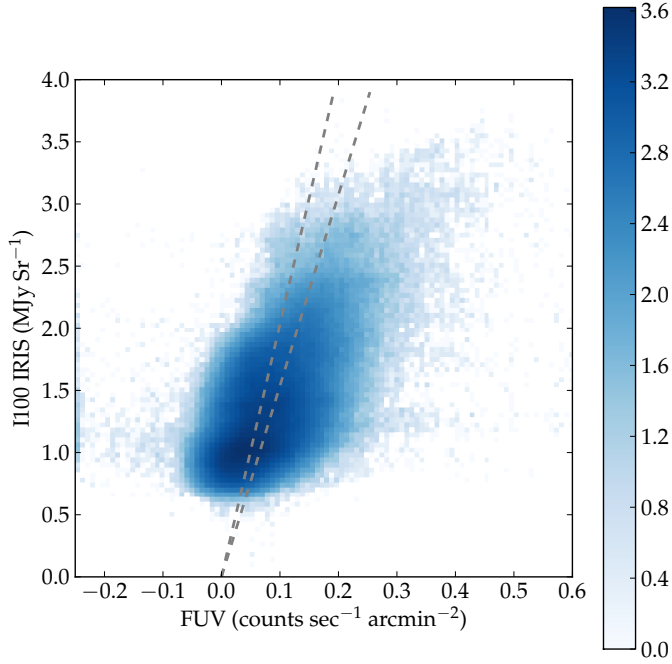
Fig. 7. FUV counts vs. 100 micron intensity diagram (I100). The colour scale shows the logarithm of the numbers of pixels within 2D-bins. The grey lines indicate the slope found by Hamden et al. (2013) for two Galactic latitudes corresponding to the GUViCS area. The maps used have 1 arcmin size pixels and have been median-filtered over 3×3 pixels. The 100 microns correspond to IRIS-reprocessed IRAS data corrected on large scales as explained in Sect. 2.3.
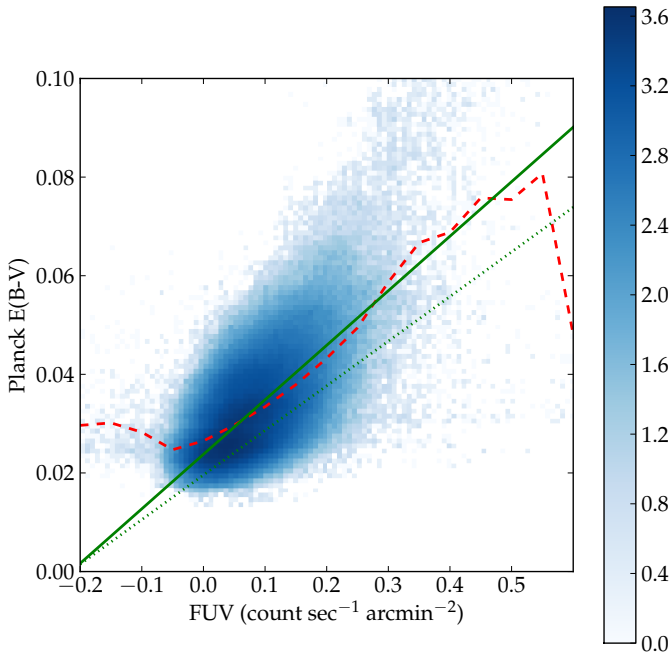

Fig. 9. Ratio of the FUV diffuse emission (in the 1 arcmin pixel map) to the 100 micron emission, after applying a Gaussian filter of 6 arcmin to both images. The contours roughly indicate the regions in which the cirrus emission is found (Sect. 3.2).

Fig. 8. *Planck* $E(B - V)$ vs. FUV counts. The colour bar indicates the logarithm of the number of pixels within each 2D-bins. The dashed line shows averages within FUV flux bins. The solid line indicates a simple linear fit to the average trend. The dotted line indicates the result of a similar analysis based on the Schlegel et al. (1998) $E(B - V)$ map.

Fig. 10. Combination of the FUV emission (blue) and 100 micron emission (red) along an extended cirrus feature, spreading from the left to the right of the figure. The scaling was chosen to show the complementarity of the two dust tracers, since the colour is changing along the structure.

to distinguish the relative performances of the various reddening maps since the dispersion in the colour of galaxies (linked to their star formation histories, metallicities, ages, and redshift) is much greater than the reddening trend itself. The observed variation in the NUV − i colour with $E(B - V)$ is consistent with the one predicted simply with this Milky Way extinction law, suggesting that the various extinction tracers provide a similar level of accuracy.

Looking into the details, however, we see in Fig. 11 that the dispersion of the colour at a given $E(B - V)$ depends slightly on the source of dust reddening considered. The one derived from the FUV 20 arcsec map is smaller than the other ones by about ten percent. The dispersion of the NUV − i colour of background galaxies in this diagram has two components: one is the intrinsic spread of colours of galaxies (due to their various star formation histories, metallicity, redshift) that is the same in each cases. The other one is obviously the incorrect assignment of the Galactic
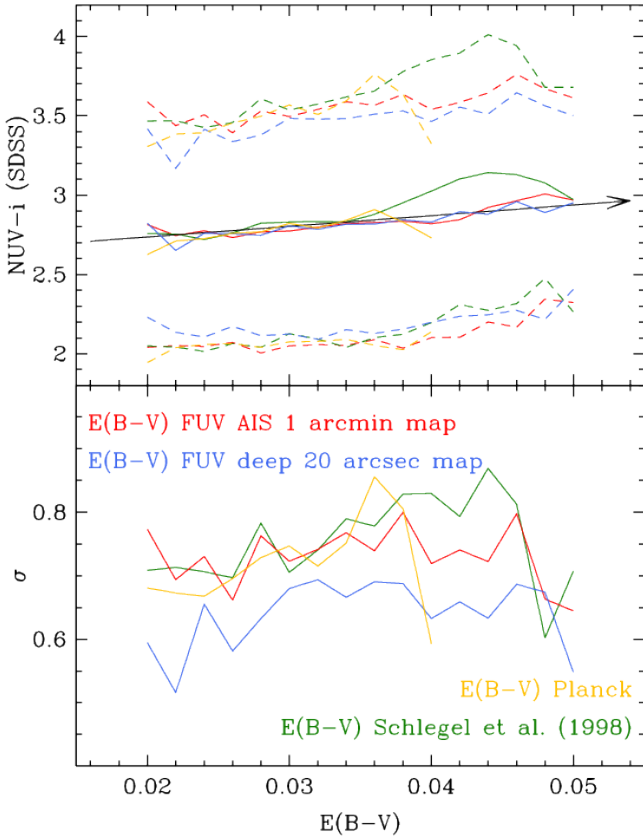
At least statistically, using the $E(B - V)$ derived from the FUV produces the expected trend on the colour, based on a Milky Way extinction curve (Cardelli et al. 1989) with $A(NUV) = 8.74 E(B - V)$ and $A(i) = 1.98 E(B - V)$. It is hard

Fig. 11. *Top*: NUV − *i* colour of SDSS galaxies in the Voyer et al. (2014) catalogue as a function of the Galactic dust reddening (taking only objects with signal-to-noise higher than 10). The solid lines show the average, while the dashed lines indicate the 1-sigma dispersion. The dust reddening is derived either from the Schlegel maps (as given in the GUViCS catalogue), from the *Planck* $E(B − V)$ map, or from our FUV 1 arcmin or 20 arcsec resolution diffuse emission maps. The arrow indicates the expected reddening trend (see Sect. 3.6). *Bottom*: the 1-sigma dispersion of the NUV − *i* colour is indicated as a function of the reddening. The range plotted in both panels corresponds to the bins where we do obtain $E(B − V)$ values for each method.

attenuation, which is changing depending on the dust tracer chosen. The "best" $E(B − V)$ estimator should produce the smallest dispersion in this figure. (For a perfect estimator, we would be left only with the dispersion intrinsic to galaxies.) We can thus conclude that the $E(B − V)$ derived from the FUV 20 arcsec map does a better job statistically for our sample than the other ones, although the difference is small. We verified that this result is not due to the smaller area covered by this mosaic, and repeating the exercise on the 1 arcmin map restricted to the area used in the 20 arcsec study does not reduce its dispersion. We thus have to attribute this better result to the resolution and depth gain when using the 20 arcsec pixel FUV map to estimate $E(B − V)$.

Some caution should be taken when using this attenuation estimator. While we found that the diffuse FUV light correlates with $E(B − V)$, and we use this to "calibrate" the reddening, it is clear that the FUV scattered light does not provide information on small-grain absorption in FUV. Moreover, recent works suggest large variability in the dust properties at high Galactic latitudes (Ysard et al. 2015). Peek & Schiminovich (2013) hint, in addition, at deviations from the standard extinction curve in the FUV band. Deriving extinctions in the FUV band from our estimate may thus produce erroneous results.

4. Conclusion

We characterised the diffuse FUV emission in the Virgo cluster direction with the GUViCS data. We compared this emission (geometrically and statistically) to the NUV emission, IRIS 100 micron emission, HeViCS 250 micron emission, and $E(B − V)$ from Schlegel et al. (1998) and from the Planck collaboration. Cirrus are clearly detected in the FUV channel. They are characterised by a constant blue FUV-NUV ∼ 0 colour. (An observed trend with FUV surface brightness is, in fact, related to observational limits.)

We find overall agreement between the locations of cirrus seen in FUV with those from other tracers, although some distinctions are found: certain regions are visible in the FUV maps but do not appear obviously in the infrared or *Planck* maps and vice versa. Despite these regions, a correlation is found when the various cirrus indicators are compared on a pixel basis (with, however, large dispersion). The FUV reveals details in the structure of the cirrus that are not always seen at any other wavelength, owing to good spatial resolution and sensitivity, but also to a complementary between the FUV and far infrared emission.

The diffuse FUV emission maps produced in this work may be useful for many purposes:

- The study of the dust properties in the UV (albedo, scattering) or the properties of cirrus in general with multi-wavelength maps matched at the same pixel size. For instance, a small region with both deep FUV data and good quality WISE W3 dust emission is shown in Fig. 12. The good agreement between the two tracers could confirm that the 12 micron emission comes from small grains and PAHs, which absorb the FUV radiation.

- In conjunction with deep optical data, the study of the extended red emission phenomenon.

- Identification of regions "polluted" by faint structures related to Galactic cirrus. This could be very useful for exploiting the surveys that have been rencently done in the Virgo area, especially NGVS in the optical and GUViCS in the UV. We further illustrate this point in Fig. 12 by showing a comparison of the same area in our FUV diffuse map and in a deep *g*-band NGVS image. (The brightest cirrus feature here reaches 27.2 mag arcsec^{-2}.) This figure shows that the cirrus are also detected in these deep high-quality optical images, owing to efficient restoration of the true sky background of MegaCam data. The similar distribution of the structures at both wavelengths confirms that it is related closely to cirrus.

- Alternative Galactic extinction estimation by using the correlation found between the diffuse FUV emission (as measured in the map we deliver) and the reddening, as detailed in sect. 3.5. The 20 arcsec FUV diffuse emission is slightly better than other dust tracers based on the relation between $E(B − V)$ and the NUV − *i* colour of background galaxies (Sect. 3.6).

While there is certainly a lot of analysis and understanding still needed, we put these FUV maps (the 1 arcmin pixels based on the AIS, and the 20 arcsec pixels based on deeper data) on the GUViCS web site[5] for this reason and made them publicly available. We also make available the complementary maps on the same 1 arcmin pixel scale as was prepared and used for our analysis.
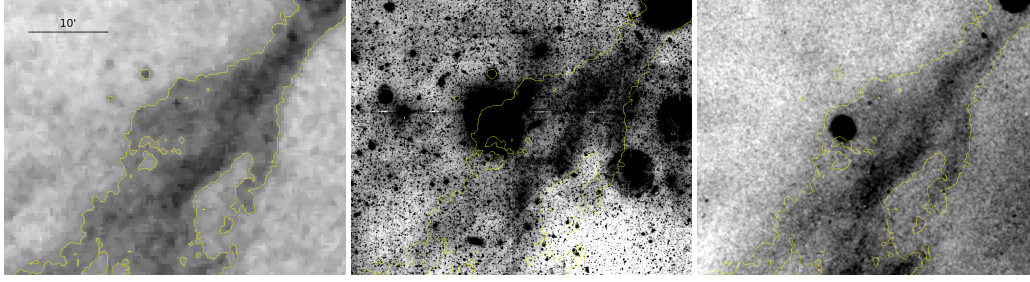
---

[5] http://galex.lam.fr/guvics/mosaics.html

Fig. 12. Region around coordinates RA = 12:36:07.201, Dec = +14:16:39.98 is shown as seen in the 20 arcsec pixels FUV diffuse light map (*left*), in the NGVS (Ferrarese et al. 2012) *g* band image (*middle*), and in the WISE W3 diffuse emission (*right*) from Meisner & Finkbeiner (2014) on the same scale. To ease the comparison, a single contour was computed in FUV and overlaid on the other images.

References

Arrigoni Battaia, F., Gavazzi, G., Fumagalli, M., et al. 2012, A&A, 543, A112
Baes, M., Herranz, D., Bianchi, S., et al. 2014, A&A, 562, A106
Boissier, S., Gil de Paz, A., Boselli, A., et al. 2007, ApJS, 173, 524
Boissier, S., Gil de Paz, A., Boselli, A., et al. 2008, ApJ, 681, 244
Boissier, S., Boselli, A., Duc, P.-A., et al. 2012, A&A, 545, A142
Boselli, A., Boissier, S., Heinis, S., et al. 2011, A&A, 528, A107
Boselli, A., Voyer, E., Boissier, S., et al. 2014, A&A, 570, A69
Bonnarel, F., Fernique, P., Bienaymé, O., et al. 2000, A&AS, 143, 33
Burstein, D., & Heiles, C. 1978, ApJ, 225, 40
Burstein, D., & Heiles, C. 1982, AJ, 87, 1165
Cardelli, J. A., Clayton, G. C., & Mathis, J. S. 1989, ApJ, 345, 245
Cortese, L., Bendo, G. J., Isaak, K. G., Davies, J. I., & Kent, B. R. 2010, MNRAS, 403, L26
Cortese, L., Catinella, B., Boissier, S., Boselli, A., & Heinis, S. 2011, MNRAS, 415, 1797
Cuillandre, J.-C., Lequeux, J., Allen, R. J., Mellier, Y., & Bertin, E. 2001, ApJ, 554, 190
Davies, J. I., Baes, M., Bendo, G. J., et al. 2010, A&A, 518, L48
de Vaucouleurs, G. 1955, The Observatory, 75, 129
de Vries, C. P., & Le Poole, R. S. 1985, A&A, 145, L7
Duc, P.-A., Cuillandre, J.-C., Karabal, E., et al. 2015, MNRAS, 446, 120
Durrell, P. R., Côté, P., Peng, E. W., et al. 2014, ApJ, 794, 103
Ferrarese, L., Côté, P., Cuillandre, J.-C., et al. 2012, ApJS, 200, 4
Fix, J. D., Craven, J. D., & Frank, L. A. 1989, ApJ, 345, 203
Frey, A., Hofmann, W., & Lemke, D. 1977, A&A, 54, 853
Fukugita, M., Yasuda, N., Brinkmann, J., et al. 2004, AJ, 127, 3155
Giovanelli, R., Haynes, M. P., Kent, B. R., et al. 2005, AJ, 130, 2598
Gondhalekar, P. M., Phillips, A. P., & Wilson, R. 1980, A&A, 85, 272
Gordon, K. D., Witt, A. N., & Friedmann, B. C. 1998, ApJ, 498, 522
Guhathakurta, P., & Cutri, R. M. 1994, The First Symposium on the Infrared Cirrus and Diffuse Interstellar Clouds, 58, 34
Guhathakurta, P., & Tyson, J. A. 1989, ApJ, 346, 773
Haikala, L. K., Mattila, K., Bowyer, S., et al. 1995, ApJ, 443, L33
Hamden, E. T., Schiminovich, D., & Seibert, M. 2013, ApJ, 779, 180
Henry, R. C., Murthy, J., Overduin, J., & Tyler, J. 2015, ApJ, 798, 14
Hodges-Kluck, E., & Bregman, J. N. 2014, ApJ, 789, 131
Hurwitz, M., Bowyer, S., & Martin, C. 1991, ApJ, 372, 167
Jakobsen, P., Bowyer, S., Kimble, R., et al. 1984, A&A, 139, 481
Leinert, C., Bowyer, S., Haikala, L. K., et al. 1998, A&AS, 127, 1
Lillie, C. F., & Witt, A. N. 1976, ApJ, 208, 64
Low, F. J., Young, E., Beintema, D. A., et al. 1984, ApJ, 278, L19
Meisner, A. M., & Finkbeiner, D. P. 2014, ApJ, 781, 5
Miville-Deschênes, M.-A., & Lagache, G. 2005, ApJS, 157, 302
Morgan, D. H., Nandy, K., & Thompson, G. I. 1976, MNRAS, 177, 531
Murthy, J. 2014, Ap&SS, 349, 165
Murthy, J., Henry, R. C., Feldman, P. D., & Tennyson, P. D. 1989, ApJ, 336, 954
Murthy, J., Hall, D., Earl, M., Henry, R. C., & Holberg, J. B. 1999, ApJ, 522, 904
Pappalardo, C., Bendo, G. J., Bianchi, S., et al. 2015, A&A, 573, A129
Paresce, F., McKee, C. F., & Bowyer, S. 1980, ApJ, 240, 387
Peek, J. E. G., & Schiminovich, D. 2013, ApJ, 771, 68
Perault, M., Lequeux, J., Hanus, M., & Joubert, M. 1991, A&A, 246, 243
Planck Collaboration XIX. 2011, A&A, 536, A19
Planck Collaboration XI. 2014, A&A, 571, A11
Sandage, A. 1976, AJ, 81, 954
Sasseen, T. P., & Deharveng, J.-M. 1996, ApJ, 469, 691
Schlegel, D. J., Finkbeiner, D. P., & Davis, M. 1998, ApJ, 500, 525
Seon, K.-I., Witt, A., Kim, I.-J., et al. 2011, ApJ, 743, 188
Seon, K.-I., Witt, A. N., Shinn, J.-H., & Kim, I.-J. 2014, ApJ, 785, L18
Sujatha, N. V., Shalima, P., Murthy, J., & Henry, R. C. 2005, ApJ, 633, 257
Sujatha, N. V., Murthy, J., Suresh, R., Conn Henry, R., & Bianchi, L. 2010, ApJ, 723, 1549
Szomoru, A., & Guhathakurta, P. 1998, ApJ, 494, L93
Voyer, E. N., Boselli, A., Boissier, S., et al. 2014, A&A, 569, A124
Witt, A. N., & Schild, R. E. 1985, ApJ, 294, 225
Witt, A. N., Friedmann, B. C., & Sasseen, T. P. 1997, ApJ, 481, 809
Witt, A. N., Mandel, S., Sell, P. H., Dixon, T., & Vijh, U. P. 2008, ApJ, 679, 497
Ysard, N., Koehler, M., Jones, A., et al. 2015, A&A, 577, A110